Fundamental Studies on the Electron Penetration in Radiotherapy

Takehiro Nishidai

Department of Radiology, Kyoto University Hospital

Research Code No.: 201

Key Words: *Electron penetration, Radiotherapy*

放射線治療における電子線透過の基礎的研究

京都大学医学部附属病院放射線部

西　台　武　弘

4から32MeV 電子線の水中における透過現象を確率論的および定性的に解析することにより，放射線治療時の物理的基礎データ：path lengthと平均深さの関係，そして各深さにおけるエネルギー・スペクトル，平均角度分布，charge rate, current, 深部量百分率，ラド変換係数 C_E：を得た．ビーム・ジオメトリーは単一エネルギー，無限平面のビームが単一方向に水に入射する理想的な状態を考えた．我々の結果は，モーメント法による Kessaris の結果と比較すると，より満足すべき結果であつた．

Summary

The penetration of electron beams of energy 4 to 32 MeV in water has been theoretically investigated with a stochastics and qualitative analysis and with a view toward applications in electron-irradiation therapy. The data concerning the average penetration depth as a function of the pathlength, as well as the energy spectrum, average angular distribution, charge rate, current, flux, percentage depth dose and rad conversion factor C_E as a function of depth were obtained. The beam geometry was considered in such a way as infinite monodirectional beam was embedded in a water of infinite extent. This result was compared with a moment method result of N.D. Kessaris and other results, and it had more sufficient generality.

Introduction

In radiotherapy of high energy electrons, it is essential to have an accurate knowledge of the dose delivered at specified points in the patient. There are many reports for calculational approches in the electron penetration by various authors[1]. However the data in most of these reports have not been used in radiotherapy because the electron energy is low (below 5 MeV) and the medium is not water. N.D. Kessaris[2][3] has mathematically investigated the penetration of energy 10 to 20 MeV in water by solving the Lewis equation by the moment method under the continuous slowing-down approximation. M.J. Berger and S.M. Seltzer[4] also calculated energy and charge deposition and flux in water with mainly 20 MeV electrons by Monte Carlo methods. However, the agreement on the results of both authers is not perfect[4]. Fig. 1 shows a comparison between a moment method result of Kessaris and a Monte Carlo result of Berger pertaining to the charge rate distribution for a 20 MeV beam, and also shows our experimental data[5].

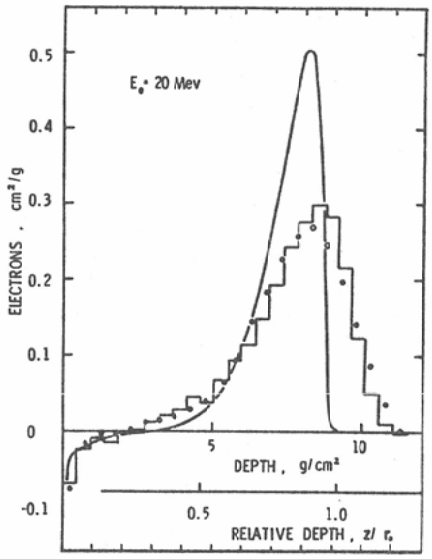

Fig. 1. Comparision between a moment method result, a Monte Carlo result and experimental data, pertaining to the charge rate distribution in water irradiated with a 20 MeV beam. Distribution is normalized to unit charge (one incident electron). Histogram is a Monte Carlo result by Berger[4]; Curve is from a moment method calculation by Kessaris[3]; Points are from our experiment[5].

The measurement in our experiment has been carried out for the current distribution by a process using the direct collection of electrons absorbed in a water phantom[5]. The charge rate distribution has been obtained from the current data. The beam in our experiment was nearly monochromatic. However, it was not perfect because of the presence of unavoidable scattering materials, such as a window of a beryllium film in 0.3 mm thick at the outlet of the accelerated electrons, and a monitor consisting of five sheets of alminium leaves in 0.02 mm thick. Our experimental results agreed well with a Monte Carlo result of Berger rather than a moment method result of Kessaris.

This theoretical treatment on the penetration of electrons will be done with a stochastics and qualitative analyses in multiple scattering, secondary electron emission and bremsstrahlung emission. This paper presents information of the penetration of 4 to 32 MeV electrons into a water phantom, according to the pioneering work of Kessaris[2][3][6] in radiotherapy. The energy range which we chose in this theoretical treatment can be produced by the betatron in Kyoto Univ. Hospital[7]. The incident beam is monoenergetic, monodirectional and broad, and it is embedded in water of infinite extent.

Theory and calculation results

1. The number of collisions

The number of electrons in a medium is changed by multiple scattering. This phenomena are applied to three physics conceptions: a) it is non-continuous process; b) each collision occurs independently; c) at least n_0

collisions are necessary to stop an initial electron: The probability that an electron has n collisions in t path length, $P(n,t)$, is expressed by a Poisson distribution.

$$P(n,t)=e^{-vt}\cdot\frac{(vt)^n}{n!} \qquad (n\neq 0) \qquad (1)$$

$$=e^{-vt} \qquad (n=0) \qquad (2)$$

where v is the average number of collisions in a unit path length (cm^2/g), t is the path length of an electron (g/cm^2), and vt is the average number of collisions which are made by one electron in t path length. Since an electron makes a large number of collisions in traversing a fraction of its path length and vt value is large, the Poisson formula (1) (2) is evaluated numerically by Gaussian distribution.

$$P(n,t)=\frac{1}{\sqrt{2\pi vt}}\cdot e^{-\frac{(n-vt)^2}{2vt}} \qquad (n\neq 0) \qquad (3)$$

$$=\frac{1}{\sqrt{2\pi vt}}\cdot e^{-\frac{vt}{2}} \qquad (n=0) \qquad (4)$$

2. The energy loss

Since vt value is large, it is possible to describe the energy loss of electrons with reasonable accuracy by continuous slowing down approximation. The energy loss per one collision in water, ΔE, is refered to the energy loss per unit path length, $-(dE/dt)$, as the total stopping power, $(s/\rho)_{E,W}$. The electron energy, E_k, with which a particle is scattered k times is given by

$$E_k=E_{(k-1)}-\Delta E \qquad (5)$$

$$=E_{(k-1)}-\frac{(s/\rho)_{E(k-1),W}}{v} \qquad (6)$$

where $(k\text{-}1)$ is reffered to the $(k\text{-}1)$th collision.

By the use of approximate slowing down model, the relationship between the electron path length and its residual energy can be obtained[8]. However, this relationship is not defined unique since electrons experience discrete and sometimes large energy losses as they traverse a material. This deviation of the energy loss of the electrons from the average is known as straggling[9]. For straggling, we shall denote the distribution of the energy loss of electrons by a simple exponential curve with extensive simplification rather than by Gaussian curve[1]. This distribution is given by

$SF(\Delta E)$

$$SF(\Delta E)=\frac{N_{\Delta E}}{N_{\Delta E_p}} \qquad (7)$$

$$=e^{-\frac{\Delta E-\Delta E_p}{\Delta E_{av}-\Delta E_p}} \qquad (8)$$

where ΔE_p is the most probable energy loss, ΔE_{av} is the average energy loss, and $SF(\Delta E)$ is a straggling factor on ΔE energy loss. This factor is expressed by the ratio of the number of electrons, $N_{\Delta E}$, *with* ΔE energy loss to the number of electrons, $N_{\Delta E_p}$, with ΔE_p energy loss. In the text book by Segré[9], ΔE_p and ΔE_{av} have been given by

$$\Delta E_p=\frac{2\pi Ne^4zx}{m_0c^2}\cdot\left(\log\frac{x}{a_0}-0.37\right) \qquad (9)$$

$$\Delta E_{av}=\frac{2\pi Ne^4zx}{m_0c^2}\cdot\left(\log\frac{E^3}{2m_0c^2I^2}+\frac{1}{8}\right) \qquad (10)$$

However, since these formulas (9) (10) are not exact, ΔE_p and ΔE_{av} in water are obtained by using the ratio of (9) and (10), and $(s/\rho)_{E,W}$.

$$\Delta E_p = \frac{\log\frac{x}{a_0} - 0.37}{\log\frac{E^3}{2m_0c^2I_{H_2O}^2} + \frac{1}{8}} \cdot \frac{(s/\rho)_{E,W}}{v} \tag{11}$$

$$\Delta E_{av} = \frac{(s/\rho)_{E,W}}{v} \tag{12}$$

From formulas (5), (8), (11), (12), the electron energy with k th collision is given by

$$E_k(SF) = E_{(k-1)} - \Delta E(SF) \tag{13}$$

$$= E_{(k-1)} - \frac{(s/\rho)_{E(k-1),W}}{v} \cdot \left\{ \frac{\log\frac{1}{va_0} - 0.37}{\log\frac{E_{(k-1)}^3}{2m_0c^2I_{H_2O}^2} + \frac{1}{8}} - \log SF \cdot \left(1 - \frac{\log\frac{1}{va_0} - 0.37}{\log\frac{E_{(k-1)}^3}{2m_0c^2I_{H_2O}^2} + \frac{1}{8}}\right)\right\} \tag{14}$$

where a_0=0.52917×10^{-8}cm[9] (Bohr radius)

m_0c^2=0.510976 MeV[8] (rest energy of a electron)

I_{H_2O}=65.1 eV[8] (mean excitation energy for water)

In this calculation, SF has been changed from 1.00 to 0.05 at intervals 0.05.

3. The scattering angle

As electrons traverse a scattering medium, their energy are lost by multiple interactions, but also they are deflected laterally from their original paths as they make multiple discrete changes in direction. These deflections are to be the results of a single scattering, multiple scattering and plural scattering[9]. The analytical treatment of this process is difficult without extensive simplification. Therefore, we think of a particle being scattered a certain number of times, k, after which it has the average direction, $\bar{\theta}_k$. For the calculation of $\bar{\theta}_k$, it is assumed that the average collision number, $m(\bar{\theta}_{sp,k})$, of a single scattering and the plural scattering at the k th collision are given by

$$m(\bar{\theta}_{sp,k}) = \frac{a(E_{(k-1)} - E_k)}{E_k^2} \tag{15}$$

where $\bar{\theta}_{sp,k}$ is the average angle for a single scattering and the plural scattering at the k th collision, and it is larger than an angle $\bar{\theta}_1$[9], and a is a constant value. This probability for a single scattering and a plural scattering is independent from the probability for the multiple scattering. The values of angle $\bar{\theta}_m$ for the multiple scattering have been recommended by ICRU[10].

The path length in a medium is not equal to the depth because of the multiple scattering of the electron. The depth, $x(n)$, in which an electron has n collisions is approximated as follows

$$x(n) \fallingdotseq \sum_{k=0}^{n-1} \{t_k(\cos\bar{\theta}_k)!\} \tag{16}$$

where t_k is the path length with k th collision. By using the average path length at each collision, $t(n)/n$, the formula (16) is given by

$$x(n) \fallingdotseq \frac{t(n)}{n} \sum_{k=0}^{n-1} \{(\cos \bar{\theta}_k)!\} \tag{17}$$

The relation between the depth, $x(n)$, and the path length, $t(n)$, is given by the formula (17). From (3), (4) and (17), we can get the probability that an electron has n collisions in $x(n)$ depth.

$$P(n,x) = \frac{1}{\sqrt{2\pi v \frac{x(n)}{b(n)}}} \cdot e^{-\frac{\left(n-\frac{vx(n)}{b(n)}\right)^2}{2v\frac{x(n)}{b(n)}}} \qquad (n \neq 0) \tag{18}$$

$$= \frac{1}{\sqrt{2\pi v x(n)}} \cdot e^{-\frac{vx(n)}{2}} \qquad (n = 0) \tag{19}$$

where

$$b(n) = \frac{1}{n} \sum_{k=0}^{n-1} \{(\cos \bar{\theta}_k)!\} \qquad (n \neq 0) \tag{20}$$

$$= 1 \qquad (n = 0) \tag{21}$$

The average penetration depth, $\langle x \rangle_{av}$, in which an electron with a path length, $t(n)$, has reached is given by

$$\langle x \rangle_{av} = \frac{\sum_{k=0}^{n_0-1} \{P(n,t) \cdot t(n) \cdot b(n)\}}{\sum_{k=0}^{n_0-1} P(n,t)} \tag{22}$$

In Fig. 2, our calculation result of the average penetration depth, $\langle x \rangle_{av}$, as a function of the path length, $t(n)$, is shown for E_o=20 MeV. E_o is the electron energy at the surface of a water medium and is called as the initial electron energy.

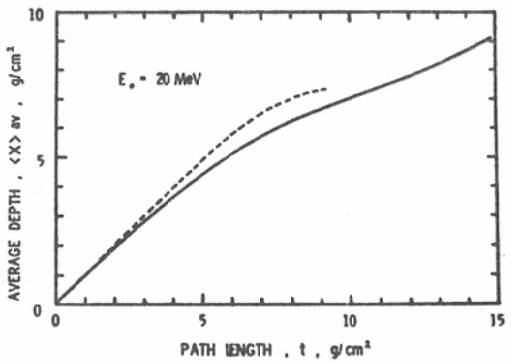

Fig. 2. The average penetration depth, $\langle x \rangle_{av}$, as a function of the path length, $t(n)$, for initial electron energy E_o=20 MeV in water. Solid curve is from the present work, and the dotted curve from a moment method calculation by Kessaris[5].

4. The primary electron distribution

We shall denote the number of the incident electrons by N_o. In this paper it is normalized with one incident electron (N_o=1). From (18), (20), the charge rate $Q_{pri}(x)$ and current $I_{pri}(x)$, for that the primary electrons are stopped at x depth to a plane surface in water, are given by

$$Q_{pri}(x) = N_0 \cdot P(n_0, x) \tag{23}$$

$$I_{pri}(x) = -\int_0^x Q_{pri}(x)\, dx \tag{24}$$

The values of n_o and m are unknown. In this calculation, we used the fitting method by using the experimental data[5] and Berger's result[4] for the charge rate distribution of the initial energy 20 MeV. (see Table 1 and Fig. 10) This method is the only fruitful one. The n_o value is calculated from the v value, and v is changed with SF. We got v value at SF=1.0 by using the fitting method.

$$v = 17.0 \qquad (\text{at } SF = 1.0) \tag{25}$$

In this calculation, v value was changed with SF value from 17.0 to 49.0 for the initial electron energy E_o=20 MeV. The value of n_o depends on v and $(s/\rho)_{E,W}$. We got n_o value with E_o approximately.

$$n_0 \fallingdotseq 9.0 \cdot E_0^{1.227-0.0394 \ln E_0} \tag{26}$$

The m value depends on a and $\bar{\theta}_{sp,k}$ values. In this calculation, since $\bar{\theta}_{sp,k}$ was used as a constant value ($\bar{\theta}_{sp,k}$=30°), we got a=4.0 by using the fittng method.

The charge rate distribution and the current distribution for E_o=20 MeV are plotted in Fig. 3 and Fig. 4, respectively.

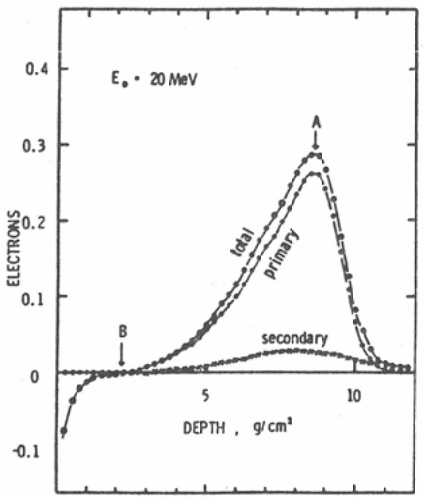

Fig. 3. The rate of charge accumulation as a function of the depth in water for initial electron energy E_o=20 MeV. The total rate which is the sum of the primary rate and the secondary rate is seen to become negative for small depths. The point A and B are respected to the peak position and the polarity altering point on the total distribution.

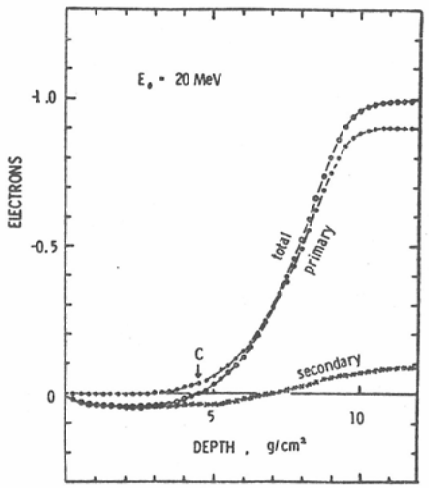

Fig. 4. The current distribution as a function of the depth in water for initial electron energy E_o=20 MeV. The total current is the sum of the primary current and the secondary current. The point C is respected to the polarity altering point on the total distribution.

The fluence, Φ, of particles is defined as quotient of dN by da[11].

$$\Phi = \frac{dN}{da} \tag{27}$$

where dN is the number of particles which enter a sphere cross-sectional area da of a volume element. For a parallel broad beam, this definition reduces to the quotient of the number of particles crossing a plane surface perpendicular. The primary electron spectrum, that is distribution of the primary electron number in energy, at depth x to this plane surface. $N_{\mathrm{pri},E}(x)$, is given by

$$N_{\mathrm{pri},E}(x) \fallingdotseq N_0 \cdot P(k,x) \tag{28}$$

The energy spectra of the primary electrons for E_o=20 MeV in water are plotted in Fig. 5. The distributions of the most probable energy[10], $(E_p)_x$, and the mean energy[10], $(\bar{E})_x$, of the spectrum for E_o=20 MeV in water are plotted in Fig. 6. The flux of the primary electrons at depth x, $\Phi_{\mathrm{pri}}(x)$, is given by

$$\Phi_{\mathrm{pri}}(x) = \int_0^E N_{\mathrm{pri},E}(x)\, dE \tag{29}$$

$$\fallingdotseq N_0 \sum_{k=0}^{n_0} P(k,x) \tag{30}$$

The flux distribution of the primary electrons for E_o=20 MeV in water is plotted in Fig. 7.

The average angular distribution of the primary electron, $N_{\mathrm{pri},\bar{\theta}_k}(x)$, is given by

$$N_{\mathrm{pri},\bar{\theta}_k}(x) \fallingdotseq N_0 \cdot P(k,x) \tag{31}$$

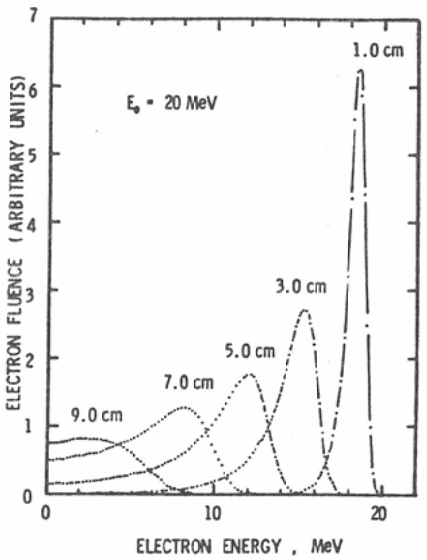

Fig. 5. The energy spectrum of primary electrons at varous indicated depths of penetration in water. The initial electron energy is 20 MeV.

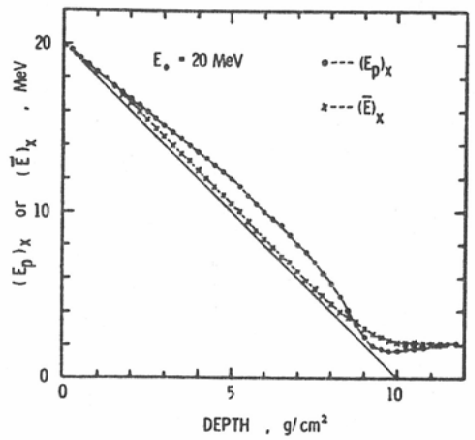

Fig. 6. Decrease of the most probable energy, $(E_p)_x$, and mean energy, $(\bar{E})_x$, with the depth in water. The straight line is from the relation[10]; $(\bar{E})_x = E_o(1-x/R_p)$, where R_p is the practical range. The initial electron energy is 20 MeV.

These distributions for E_o=20 MeV in water are plotted in Fig. 8.

The absorbed dose, D, is defined as the quotient of $d\epsilon$ by dm[11)]

$$D=\frac{d\bar{\epsilon}}{dm} \tag{32}$$

where $d\epsilon$ is the mean energy imparted by ionizing radiation to the mater in a volume element and dm is the mass of the matter in that volume element. The depth dose at depth x in water for the primary electrons, $D_{\mathrm{pri}}(x)$, is closely approximated by [10)]

$$D_{\mathrm{pri}}(x)=\int_{\Delta}^{E_0} N_{\mathrm{pri},E}(x)\cdot(S/\rho)_{E,\mathrm{col},\Delta,w}\,dE \tag{33}$$

where $(S/\rho)_{E,\mathrm{col},\Delta,w}$ is the restricted collision mass stopping power in water for electrons of energy E. The formula (33) is written by

$$D_{\mathrm{pri}}(x)\fallingdotseq\sum_{k=0}^{n_0}\left(N_0\cdot P(k,x)\cdot\frac{(S/\rho)_{k,\mathrm{col},\Delta,w}}{v}\right) \tag{34}$$

In this calculation, the cut off energy Δ was used as Δ=10 keV and the electron energy was calculated from the formula (14). The depth dose distribution of the primary electrons for E_o=20 MeV is plotted in Fig. 9.

5. The secondary electrons

The assumption that fast (primary) electrons continuously dissipate their energy is invalid because large energy transfers to atom give rise to the projection of secondary electrons in electron-electron knock-on collisions. However, due to relatively short electron ranges, the part of the spectrum below 10 keV of secondary

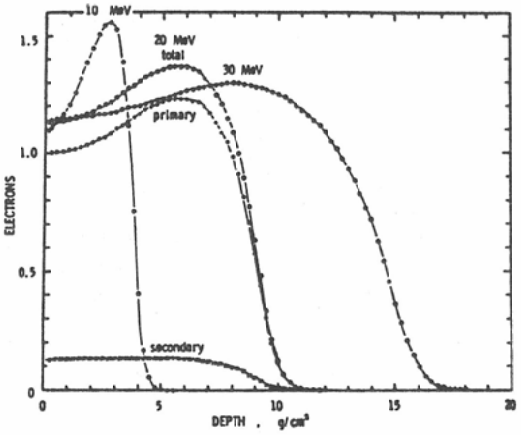

Fig. 7. The flux distributions as a function of the depth in water with initial electron energy E_o=10, 20, 30 MeV. The total flux is the sum of the primary flux and the secondary flux. Distribution is resulting from an incident current of one electron.

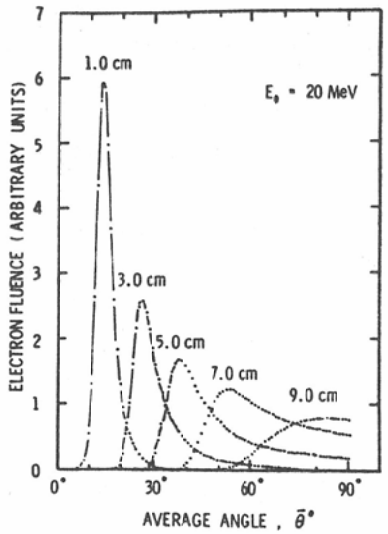

Fig. 8. The average angular distribution of the primary electron at various indicated depths of penetration in water. The initial electron energy is 20 MeV.

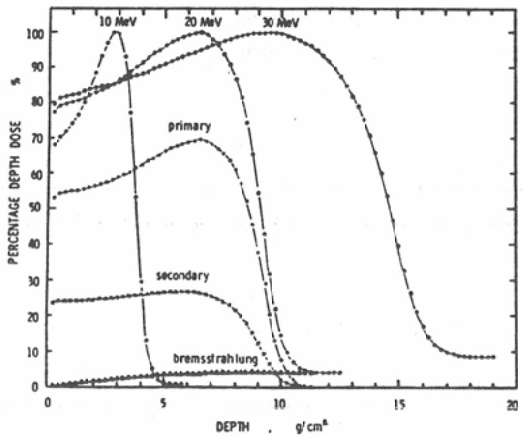

Fig. 9. The percentage depth dose distributions with initial electron energy E_o=10, 20, 30 MeV in water.

electrons may be easily attenuated at the given depth. For this reason, the cut off energy Δ in this paper is used as Δ=10 keV. The total energy of secondary electrons at the k th collision of a primary electron, $E_{s,k}$, is given by

$$E_{s,k} = \frac{(s/\rho)_{k,\mathrm{col},E/2,w} - (s/\rho)_{k,\mathrm{col},\Delta,w}}{v} \tag{35}$$

where $(s/\rho)_{k\,\mathrm{col},E/2,w}$ is the collision mass stopping power in water.

For the secondary electron, we use the assumptions that, a) m number of secondary electrons is emitted on one collision of the primary electrons, and the number, $N_{s,k,m}(x)$, and the average energy, $\bar{E}_{s,k,m}(x)$, of the secondary electrons at the depth x are given by

$$N_{s,k,m}(x) = N_{\mathrm{pri},k}(x)\cdot m \tag{36}$$

$$\bar{E}_{s,k,m}(x) = \frac{E_{s,k}(x)}{m} \tag{37}$$

b) the δ rays emitted by the secondary electrons do not contribute much to the total distribution; c) the path length of the secondary electrons is expressed by the c.s.d.a. range[3], $r_o(\bar{E}_{s,k,m})$,; d) the scattering angle of the secondary electron, $\bar{\theta}_{s,k,m}$ is given by the next approximated formula.

$$\cos\bar{\theta}_{s,k,m} = \cos\bar{\theta}_k\cdot\sqrt{\frac{\bar{E}_{s,k,m}}{\bar{E}_k}} \tag{38}$$

From these assumptions, we have calculated the secondary (electron) distributions. The charge rate, $Q_s(x)$, and current, $I_s(x)$ of the secondary electrons in water are given by

$$Q_s(x) = \sum_{k=1}^{n_0}\{N_{s,k,m}(x - r_0(\bar{E}_{s,k,m})\cdot\cos\bar{\theta}_{s,k,m}) - N_{s,k,m}(x)\} \tag{39}$$

$$I_s(x) = -\int_0^x Q_s(x)\,dx \tag{40}$$

where $N_{s,k,m}(x-r_o(\bar{E}_{s,k,m})\cdot\cos\bar{\theta}_{s,k,m})$ is the number of the secondary electrons that is emitted at the depth $(x-r_o(\bar{E}_{s,k,m})\cdot\cos\bar{\theta}_{s,k,m})$, and it is minus charge rate. $N_{s,k,m}(x)$ is the number of the secondary electrons are emitted at the depth x, and it is plus charge rate. In this calculation, we got m value by using the fitting method.

$$m=0.15 \tag{41}$$

The secondary charge rate distribution and the secondary current distribution for E_o=20 MeV are plotted in Fig. 3 and Fig. 4, respectively.

The flux of the secondary electron at depth x in water, $\Phi_s(x)$, is given by

$$\Phi_s(x)=\sum_{k=1}^{n_0}\left(\frac{r_0(\bar{E}_{S,k,m})}{v}\cdot N_{S,k,m}(x)\right) \tag{42}$$

and this distribution for E_o=20 MeV is plotted in Fig. 7.

The depth dose of the secondary electrons at the depth x in water, $D_s(x)$, is given by

$$D_S(x)=\int_0^{E_0} N_{S,E,m}(x)\cdot(S/\rho)_{E,\mathrm{col},A,w}\,dE \tag{43}$$

Since $\bar{E}_{s,k,m}(x)$ calculated from the formula (37) distribute below about 0.26 MeV for initial energy 1 to 32 MeV and the δ rays do not contribute to the distribution, the formula (43) is closely approximated by

$$D_s(x)=\sum_{k=1}^{n_0}\{n_0\cdot P(k,x)\cdot E_{S,k}\} \tag{44}$$

The depth dose distribution of the secondary electrons calculated with the formula (44) is plotted for E_o=20 MeV in Fig. 9. The contribution by the secondary electrons on the total depth dose changes from about 24% on the surface to 30% on the peak depth for the initial electron energy 20 MeV.

6. The bremsstrahlung photons

The total energy of bremsstrahlung photons emitted at the k th collision of a primary electron, $E_{B,k}$, is given by

$$E_{B,k}=\frac{(S/\rho)_{k,\mathrm{Rad},w}}{v} \tag{45}$$

where $(S/\rho)_{k,\mathrm{Rad},w}$ is the mass stopping power for energy loss due to bremsstrahlung production in water. The spectral distributions of bremsstrahlung photons with energy are continuous. However in this paper, we assume that the photon energy can be expressed by the monoenergy, E_k, of the primary electrons at k th collision that is given by the formula (14) with extensive simplification. The depth dose of bremsstrahlung photons that are produced at the k th collision of a primary electron, $D_{B,k}(x)$ is approximated by

$$D_{B,k}(x)\fallingdotseq\int_0^x(\mu_{en}/\rho)_{E_k,w}\cdot E_{B,k}\cdot N_{\mathrm{pri},k}(x)\cdot e^{-(\mu/\rho)_{E_k w}\cdot x_1}\,dx \tag{46}$$

where $(\mu_{en}/\rho)_{E_k,w}$ and $(\mu/\rho)_{E_k,w}$ are the mass absorbtion coefficient and the mass attenuation coefficient of water for a photon with E_k energy respectively, and x_1 is the distance from the point where a photon is produced to the point of depth x. The total depth dose of bremsstrahlung photons at depth x, $D_B(x)$, is given by

$$D_B(x)=\sum_{k=0}^{n_0} D_{B,k}(x) \tag{47}$$

$$=\sum_{k=0}^{n_0}\left(\int_0^x (\mu_{en}/\rho)_{E_k,w}\cdot E_{B,k}\cdot N_0\cdot P(k,x)\cdot e^{-(\mu/\rho)_{E_k,w}\cdot x_1}\,dx\right) \tag{48}$$

The contribution of $D_B(x)$, that was calculated, is plotted for E_o=20 MeV in Fig. 9.

7. The total distribution

The total distribution of the charge rate $Q(x)$, current $I(x)$ and flux $\Phi(x)$ are given by

$$Q(x)=Q_{\text{pri}}(x)+Q_S(x) \tag{49}$$
$$I(x)=I_{\text{pri}}(x)+I_S(x) \tag{50}$$
$$\Phi(x)=\Phi_{\text{pri}}(x)+\Phi_S(x) \tag{51}$$

These distributions for E_o=10, 20, 30 MeV are plotted in Fig. 3,4,7, respectively. The peak position A in Fig. 3, and positions B, C in Fig. 3,4 where the polarity alter in the charge rate as well as current distributions, and width at half maximum of the charge rate distribution in water are shown in Table 1 and Fig. 10.

The total distribution of the depth dose, $D(x)$, is given by

$$D(x)=D_{\text{pri}}(x)+D_S(x)+D_B(x) \tag{52}$$

And, the percentage depth dose, $D_{\text{percentage}}(x)$, is

$$D_{\text{percentage}}(x)=100\cdot\frac{D(x)}{D_p} \tag{53}$$

where D_p is a peak depth dose. The percentage depth dose distribution for E_o=10, 20, 30 MeV in water are plotted in Fig. 9, and the depth at 50, 80, 100 per cent depth dose is plotted as a function of the initial electron energy E_o in Fig. 11.

An indirect method of the initial electron energy determination is very often preferred using well established empirical relationship between the initial electron energy, E_o, and the practical range, R_p. In Fig. 11, R_p values that are obtained from the data of the percentage depth dose are shown, and that is expressed by the relations.

$$\rho\cdot R_p=0.598E_0-1.79 \qquad (10\leqq E_0\leqq 32) \tag{54}$$
$$=0.49E_0-0.65 \qquad (4\leqq E_0\leqq 10) \tag{55}$$

Table 1. Calculated and experimental parameters of the charge rate distribution for initial electron energy E_0 = 20 MeV in water

	Peak Position (g/cm²)	Full Width at Half-max (g/cm²)
This result ; calculation	8.60	3.30
Our result[5] ; experiment	8.30	3.60
Berger[4] ; calculation	8.54	3.12
Kessaris[4] ; calculation	7.99	1.74
Alexander[4] ; experiment	8.08	3.95
Laughlin[4] ; experiment	7.71	3.30

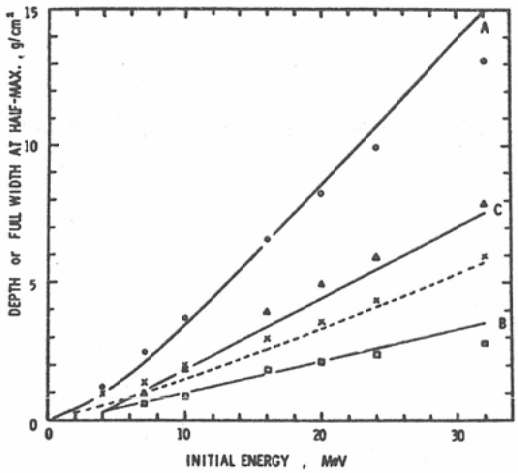

Fig. 10. The peak position A on the charge rate distribution and the positions B, C where the polarity alter on the charge rate and current distributions (see Fig. 3,4), and width at half maximum of the charge rate distribution with initial electron energy. Solid curve is from the present work and points, ○, □, △, are from our experiment[5] for A, B, C positions, respectively. The dotted curve is from the present work and point, ×, is from our experiment for width at half maximum of the charge rate distribution.

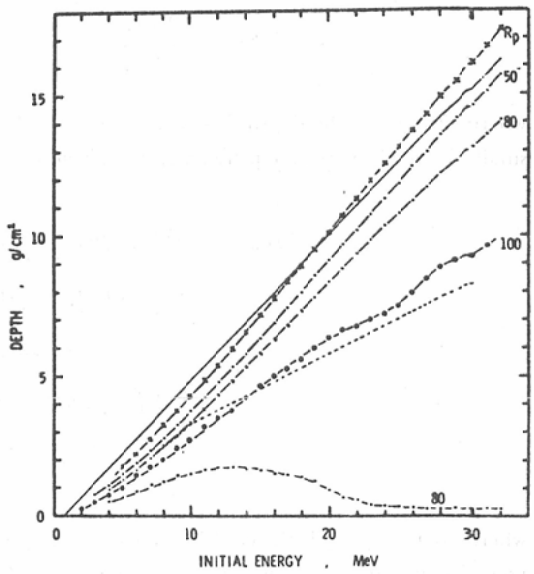

Fig. 11. The depth at 50, 80, 100 per cent depth dose and the practical range, R_p, with initial electron energy from the present work. The straight line is the recommended R_p value from the formula (74) by ICRU[10]. The dotted line is the average depth at 80 per cent depth dose from the practical therapy machines[15].

8. The conversion factor, C_E

In practical electron dosimetry, an ionization chamber calibrated as an exposure meter for high energy photons (^{60}Co or 2 MV Xrays) is available. The absorbed dose at the point of measurement in water phantom using an ionization chamber is given by[10]

$$D(x) = M(x) \cdot N_c \cdot C_E \qquad (56)$$

where $M(x)$ is the instrument reading; N_c is the exposure calibration factor and C_E is the overall conversion factor to absorbed dose in water. In ICRU Report[10], C_E is given by

$$C_E = A_0 \cdot s_{w,g} \cdot p_{w,g} \cdot \bar{w}/e \qquad (57)$$

where A_o is the attenuation factor; $s_{w,g}$ is the stopping power ratio; $p_{w,g}$ is the perturbation ratio; $\bar{w}$ is the average energy expended in the gas per ion pair formed and e is the charge of the electron. Since C_E recommended by ICRU[10] is the overall conversion factor, this value depends on the shape and the wall material of the ionization chamber, and is changed with $s_{w,g}$ and $p_{w,g}$ values. In this paper, supposing that the wall material is water and the chamber cavity is a small air-filled cavity (the Bragg-Gray Cavity), C_E values were calculated by using values of $s_{\text{water,air}}$ and by taking $p_{\text{water,air}}$=1.00. The stopping power ratio $s_{\text{water,air}}$, which is the essential constituent of the Bragg-Gray relation, is given by

$$S_{\text{water, air}} = \frac{D_{\text{water}}(x)}{D_{\text{air}}(x)} \tag{58}$$

where $D_{\text{water}}(x)$ is the depth dose $D(x)$ calculated by the formula (52), and $D_{\text{air}}(x)$ is the absorbed dose in the small air-filled cavity at depth x. $D_{\text{air}}(x)$ is given by

$$\begin{aligned} D_{\text{air}}(x) = & \sum_{k=0}^{n_0}\left(N_0 \cdot P(k,x)\cdot\frac{1}{v}\cdot(s/\rho)_{k,\text{col,air}}\right) \\ & + \sum_{k=0}^{n_0}\left(N_0 \cdot P(k,x)\cdot\frac{1}{v}\cdot\{(s/\rho)_{k,\text{col},E/2\rho,\text{air}} \right. \\ & \left. -(s/\rho)_{k,\text{col},\Delta,\text{air}}\}\right) \\ & + \sum_{k=0}^{n_0}\left(\int_0^x N_0 \cdot P(k,x)\cdot(\mu_{en}/\rho)_{E_k,\text{air}}\cdot\frac{1}{v}\right. \\ & \left. \cdot(s/\rho)_{k,\text{Rad},w}\cdot e^{-(\mu/\rho)E_k,w\cdot x_1}\,dx\right) \end{aligned} \tag{59}$$

where $(s/\rho)_{k,\text{col},E/2,\text{air}}$ is the collision mass stopping power in air; $(s/\rho)_{k,\text{col},\Delta,\text{air}}$ is the restricted collision stopping power in air; $(\mu_{en}/\rho)_{E_k,\text{air}}$ is the mass absorption coefficient of air for a photon energy with E_k. Calculated values of C_E by taking A_o=0.985, $p_{\text{water,air}}$=1.00, $\bar{w}/e$=0.869 and using formulas (57) (58) are shown in Fig. 12 for E_o=10, 20, 30 MeV and in Table 2 for E_o=4-32 MeV.

9. Approximation of $\bar{\theta}_m$, (s/ρ), r_o, (μ/ρ) and (μ_{en}/ρ)

In this study, approximate estimations of the angle for the multiple scattering, the mass stopping power, c.s.d.a. range for the secondary electron, the mass absorbition coefficient and the mass attenuation coefficient were made with the published pertinent data;

$$\bar{\theta}_m = \sqrt{3.39\cdot\rho\cdot l\cdot E^{(-0.06167\ \ln E-1.506)}+50.0\ e^{-9.78E}+833.0\,e^{-32.2E}} \tag{60}$$

With ICRV Report 21[10]

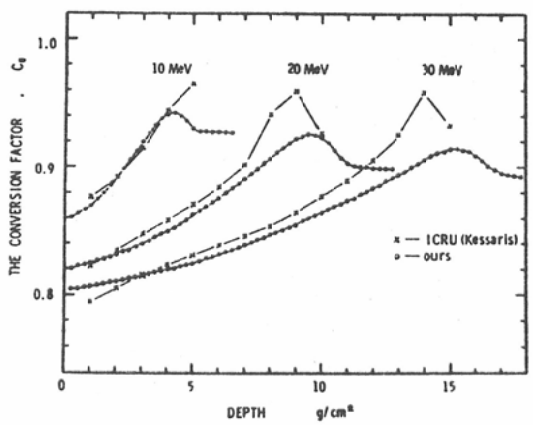

Fig. 12. Comparison of C_E values between our calculated result and a moment method result of Kessaris that is recommended by ICRU[10].

Table 2. Values for C_E in rad/R for electron beams in water

Depth in Water d/cm	Initial Electron Energy E_o/MeV																												
	4	5	6	7	8	9	10	11	12	13	14	15	16	17	18	19	20	21	22	23	24	25	26	27	28	29	30	31	32
0.5	.926	.910	.898	.887	.878	.870	.864	.857	.852	.847	.842	.838	.835	.831	.828	.825	.823	.820	.818	.816	.814	.812	.811	.809	.808	.807	.805	.804	.803
1.0	.953	.933	.914	.900	.888	.878	.870	.863	.857	.852	.847	.842	.838	.835	.831	.828	.825	.823	.821	.818	.816	.815	.813	.811	.810	.808	.807	.806	.805
1.5	.954	.951	.939	.918	.903	.890	.880	.871	.864	.857	.852	.847	.842	.838	.835	.831	.828	.826	.823	.821	.819	.817	.815	.813	.812	.810	.809	.808	.807
2.0	.955	.951	.949	.937	.920	.905	.892	.881	.872	.865	.858	.852	.847	.843	.839	.835	.832	.829	.826	.824	.821	.819	.817	.815	.814	.812	.811	.810	.809
2.5	.955	.952	.949	.947	.936	.920	.906	.893	.883	.874	.866	.859	.853	.848	.843	.839	.835	.832	.829	.827	.824	.822	.820	.818	.816	.814	.813	.812	.810
3.0		.953	.948	.947	.945	.935	.920	.906	.894	.884	.875	.867	.860	.854	.849	.844	.840	.836	.833	.830	.827	.825	.823	.820	.818	.817	.815	.814	.812
3.5			.948	.943	.944	.943	.933	.920	.906	.894	.884	.875	.868	.861	.855	.850	.845	.841	.837	.834	.831	.828	.825	.823	.821	.819	.818	.816	.814
4.0				.943	.938	.942	.941	.932	.918	.905	.894	.885	.876	.868	.862	.856	.850	.846	.842	.838	.834	.831	.829	.826	.824	.822	.820	.818	.817
4.5					.938	.934	.940	.939	.930	.917	.905	.894	.885	.876	.869	.862	.856	.851	.846	.842	.839	.835	.832	.829	.827	.825	.823	.821	.819
5.0						.933	.930	.938	.937	.928	.916	.904	.894	.885	.876	.869	.863	.857	.852	.847	.843	.840	.836	.833	.830	.828	.825	.823	.822
5.5							.928	.928	.937	.935	.926	.914	.903	.893	.884	.876	.869	.863	.858	.853	.848	.844	.840	.837	.834	.831	.829	.826	.824
6.0							.927	.923	.926	.936	.933	.924	.913	.902	.893	.884	.876	.870	.864	.858	.853	.849	.845	.841	.838	.835	.832	.829	.827
6.5								.923	.919	.925	.934	.931	.922	.911	.901	.892	.884	.876	.870	.864	.858	.854	.849	.845	.842	.838	.835	.833	.830
7.0									.919	.916	.925	.933	.929	.920	.910	.900	.891	.883	.876	.870	.864	.859	.854	.850	.846	.842	.839	.836	.834
7.5										.915	.914	.925	.931	.927	.918	.908	.899	.890	.882	.876	.870	.864	.859	.854	.850	.847	.843	.840	.837
8.0											.912	.912	.924	.930	.925	.917	.907	.897	.889	.882	.875	.870	.864	.859	.855	.851	.847	.844	.841
8.5												.909	.912	.925	.928	.923	.915	.905	.896	.888	.881	.875	.869	.864	.859	.855	.851	.848	.844
9.0													.907	.912	.924	.927	.922	.913	.904	.895	.888	.881	.875	.869	.864	.860	.855	.852	.848
9.5														.905	.912	.924	.926	.920	.912	.903	.895	.887	.880	.875	.869	.864	.860	.856	.852
10.0															.904	.912	.923	.924	.918	.910	.902	.893	.886	.880	.874	.869	.864	.860	.856
10.5																.903	.913	.922	.922	.916	.909	.900	.892	.886	.880	.874	.869	.864	.860
11.0																	.903	.914	.922	.921	.915	.907	.899	.892	.885	.874	.874	.869	.864
11.5																	.900	.903	.915	.921	.919	.913	.905	.898	.891	.884	.879	.873	.869
12.0																		.889	.904	.915	.920	.918	.912	.904	.897	.890	.884	.878	.873
12.5																			.898	.904	.915	.919	.916	.910	.903	.895	.889	.883	.878
13.0																				.898	.905	.915	.918	.915	.909	.901	.894	.888	.882
13.5																					.898	.906	.915	.917	.913	.907	.900	.893	.887
14.0																						.898	.907	.915	.916	.912	.906	.899	.892
14.5																							.899	.908	.914	.915	.911	.904	.898
15.0																								.899	.908	.914	.914	.909	.903
15.5																									.900	.908	.913	.912	.908
16.0																										.900	.909	.912	.911
16.5																											.901	.909	.912
17.0																												.902	.909
17.5																													.902

where θ_m is expressed with radian unit; ρ is the density of water ($\rho \fallingdotseq 1$); l is the path length given by $1/v$ in this paper; E is the electron energy given by the formula (14)

$$(s/\rho)_{E,\text{water}} = 0.04671|E-1.4|^{0.875}+1.866+3.0\,e^{-6.0E}+9.34\,e^{-27.0E} \quad (61)$$

$$(s/\rho)_{E,\text{col},E/2,\text{woter}} = 0.018|E-1.5|^{(e^{-0.210\ln|E-1.5|+0.457})} +1.852+1.919\,e^{-4.615E}+3.7\,e^{-12.0E} \quad (62)$$

$$(s/\rho)_{E,\text{col},E/2,\text{air}} = 0.055|E-1.3|^{(-0.115\ln|E-1.3|+1.087)} +1.650+2.826\,e^{-6.6E} \quad (63)$$

$$(s/\rho)_{E,\text{Rad,water}} = 0.013E^{1.139}+0.004 \quad (64)$$

with Berger's data[8]

$$(s/\rho)_{E,\text{col},10\,\text{KeV,water}} = 0.01\ln E+1.39+1.06\,e^{-2.47E}+5.63\,e^{-12.7E} \quad (65)$$

with ICRU Report 16[12]

$$(s/\rho)_{E,\text{col},10,\text{KeV,air}} = 0.126\ln E+1.165+1.46\,e^{-2.47E}+5.5\,e^{-15.0E} \quad (66)$$

with ICRU Report 16[12] and 14[13]

$$(s/\rho)_{E,\text{col},E'2,\text{water}}-(s/\rho)_{E,\text{col},10\,\text{KeV,water}} = 0.0799\ln E+0.396 \quad (67)$$

with Berger's data[8] and ICRU Report 16[12]

$$r_0 = 0.444\,E^{1.142-0.04385\ln E}-0.02389\,e^{-0.855|E-0.4|} \quad (E\geqq 0.3\,\text{MeV}) \quad (68)$$

$$= 0.577\,E^{1.615} \quad (E<0.3\,\text{MeV}) \quad (69)$$

with Berger's data[8]

By using these formulas (60)-(69), an accuracy is below 1% for energy 0.1 to 35 MeV.

$$(\mu/\rho)_{E,\text{water}} = 0.0162+0.00001\,E+0.0174\,e^{-0.118E} +0.0347\,e^{-0.413E}+0.0629^{-1.37E} \quad (70)$$

$$(\mu/\rho)_{E,\text{water}} = 0.0150+0.0225\,e^{-0.347E} \quad (71)$$

$$(\mu_{en}/\rho)_{E,\text{air}} = 0.0145+0.0199\,e^{-0.402E} \quad (72)$$

with NSRDS-NBS 29[14]

By using (70) (72), an accuracy is below 1% for energy 1 to 35 MeV.

Discussion

The practical circumstance of the electron beams in the betatron and the liniear accelerator are usually more complex than assumed in this calculation. However, we believe that our calculational approach may be of help to dosimetry for electron-irradiation therapy.

In this calculation, v has been used as the average number of collisions in unit path length, and this value has been obtained by using the fitting method. However, it can be considered that it is not the practical number of collisions but is only a value that decides the shape of the electron distribution. From this consideration, n_o value calculated from the formula (26) is not the practical collision number to stop an initial electron. The same discussion can be applied to a and m values. The width at half-maximum and the peak position A on the charge rate distribution depend mainly upon the values of v and a, respectively. The number of secondary electrons and the positions B and C, where the polarity alter on the change and current distribution, depend

mainly upon the m value.

The comparisons of the charge rate and current distributions in water for the initial energy of 20 MeV, that include the data on Berger's report[4] and our experimental data[5] as well as calculated values from the present work, are given in Table 1 and Fig. 10. The agreement of the present work with experimental data is not perfect, because it is very difficult to satisfy the monochromatic condition in the experiment. The comparison clearly indicates that values of Kessaris are different from other data. The reason is that in continuous-slowing down approximation on the moment method by Kessaris, it was assumed that the electrons lose energy continously along their path so that their energy is a determinstic rather than a stochastic function of the path length traversed, the energy loss at each point of their track being assumed equal to the mean loss. In this paper, we have taken into account energy-loss fluctuations (straggling). This difference is shown in Fig. 2.

The most probable energy, $(E_p)_x$, of electrons in carbon, mesured by Harder[10], decreases linealy with absorber thickness. However, $(E_p)_x$ in water, calculated in this work, does not decrease linealy. (in Fig. 6) On the contrary, the mean energy of spectrum, $(\bar{E})_x$, in water decreases linealy and is approximately expressed by the relation recomended by ICRU[10];

$$(\bar{E})_x = E_0\left(1-\frac{x}{\rho\cdot R_p}\right) \tag{73}$$

where $\rho\cdot R_p$ is the practical range given by the formula (54) (55).

Secondary electrons are produced not only as the result of a knock-on collision but also as the result of an interaction of a bremsstrahlung photon with water. In this paper we neglected the later because the contribution of bremsstrahlung photons in the depth dose is not large.

The comparison between the depth at 80 per cent depth dose obtained from our calculation and the average depth[15] at this depth dose obtained by the practical therapy machines is shown in Fig. 11. In this comparison, it is clear that such differences can be attributed to contamination of the beam by scattered electrons originating from the therapy machine and its accessories, especially the collimator device. Since the depth dose curves in electron radiotherapy show variations by scattered electrons, the own data of the depth dose curves for practical radiotherapy must be obtained by a dosimeter.

The relations between E_o and R_p in water was expressed by the formulas (54) (55). However, ICRU [10] have recommended the next formula.

$$\rho\cdot R_p = 0.521\,E_0 - 0.376 \tag{74}$$

This formula was deriven from the experimental data of Markus, B. On the other hand, Hoshino, K., et al.[16] have experimentally determined the relation between energy and R_p for 10-30 MeV electrons, and reported that the relation between $(E_p)_o$ and R_p may be approximated by a different formula, and the relations between $\bar{E}_o$ or E_a and R_p will not be given by a single formula. These difference are resulted from the beam condition, especially, from that our calculated beam condition is monoenergitic. Thus, in the practical dosimetry, this relation between energy and R_p must be used with care.

In this paper, C_E values have been calculated by using the Bragg-Gray relation. However, in practical cases the Bragg-Gray condition is not met completely and the contributions made to $D_{air}(x)$ by secondary electrons produced either in air (probe material), in the wall material of the chamber and in water (surrounding media) must be considered. It has been the aim of the cavity theory by Burlin[17] to calculate these boundary effects and thereby to drive the stopping power ratio, especially for wall-less air cavity embedded in various media. However, this theory is not perfect[18]. For practical purposes, ICRU[10] recommended two ways of suppressing

such boundary effects; a) the atomic composition of the sensitive probe material of the wall should closely resemble the composition of the material of the surrounding medium, or b) the probe wall may take over the function of suppressing boundary effects. Therefore, it can be more useful to calculate C_E values by supposing the Bragg-Gray Cavity. Fig. 12 shows the comparison of C_E values between our calculated result and a moment method result of Kessaris recommended by ICRU[10]. The agreement is good except values at large depths. Otherwise, Antoku, S., et al.[19] has experimentally determined C_E values by using a Frick dosimeter and reported that these have been also agreed with Kessaris data. However, at large depths, these were dependent on the effective center position of the chamber. There are no data at the depths deeper than r_o in Kessaris report. This difference at large depths is resulted from that Kessaris has calculated by the simplified function-fitting method with a Wick-type argument[20] at large depths.

Acknowledgement

The author is indebted to Professor Mitsuyuki Abe for his suggestions and comments in the preparation of this manuscript, and also to Professors Kanji Torizuka and Ryuhei Kato for constant encouragements

References

1) Zerby, C.D. and Keller, F.L.: Electron transport therory, Calculations and experiments. Nucl. Sci. Eng., 27: 190—218, 1967
2) Kessaris, N.D.: Calculated absorbed dose for electrons. Radiat. Res., 23: 630—640, 1964
3) Kessaris, N.D.: Penetration of high-energy electron beams in water. Phys. Rev., 145: 164—174, 1966
4) Berger, M.J. and Seltzer, S.M.: Calculation of energy and charge deposition and of the electron flux in a water medium bombarded with 20 MeV electrons. Ann. New York Acad. Sci., 161: 8—23, 1969
5) Nishidai, T., Suyama, S., Onoyama, Y. and Kato, R.: Electron charge distribution in water and saline solution. Nipp. Act. Radiol., 36: 453, 1976
6) Kessaris, N.D.: Absorbed dose and cavity ionization for high-energy electron beams. Radiat. Res., 43: 288—301, 1970
7) Fukuda, M. et al.: A new 32 MeV betatron in Kyoto University Hospital. Nipp. Act. radiol., 28: 885—886, 1968
8) Berger, M.J. and Selzer, S.M.: Tables of energy losses and ranges of electrons and positrons. NASA SP-3012 (National Aeronantics and Space Administration, Washington, D.C.), 1964
9) Segré, E.: Nuclei and particles, An introduction to nuclear and subnuclear physics: 1—58, 1965, W.A. Benjamin, Inc., New York
10) ICRU: Report 21, Radiation dosimetry: Electrons with initial energies between 1 and 50 MeV, ICRU publications, 1972, Washington, D.C.
11) ICRU: Report 19, Radiation quantities and units, ICRU publications, 1971, Washington, D.C.
12) ICRU: Report 16, Linear energy transfer, ICRU publications, 1970, Washington, D.C.
13) ICRU: Report 14, Radiation dosimetry: X-rays and gamma rays with maximum photon energies between 0.6 and 50 MeV, ICRU publications, 1969, Washington, D.C.
14) NSRD-NBS 29: Photon cross sections, Attenuation coefficients and energy absorption coefficients from 10 keV to 100 GeV: 1969, Washington, D.C.
15) JARP: Report, standard dosimetry in radiotherapy with high energy electron, 1974, Tsusyosangyosya, Tokyo
16) Hoshino, K., Inada, T. and Matsuzawa, H.: Relation between energy and practical range for 10—30 MeV electrons. Nipp. Act. Radiol., 34: 433—439, 1974
17) Burlin, T.E.: A general theory of cavity ionization. Brit. J. Radiol., 39: 727—734, 1966
18) Shiragai, A.: An approach to analysis of the energy response of LiF-TLD to high energy electron. Phys. Med. Biol., 22: 490—499, 1977
19) Antoku, S., Sunayashiki, T. and Takeshita, K.: Rad conversion factor of ionization chamber for high energy X-rays and electron. Nipp. Act. Radiol., 33: 686—688, 1973
20) Spencer, L.V.: Theory of electron penetration. Phys. Rev., 98: 1597—1615, 1955